RSC Advances

Experimental and Computational Studies on Zeolite-Y Encapsulated Iron(III) and Nickel(II) Complexes Containing Mixed-ligand of 2,2'-bipyridine and 1,10-phenanthroline

Journal:	*RSC Advances*
Manuscript ID	RA-ART-07-2015-014954.R1
Article Type:	Paper
Date Submitted by the Author:	23-Sep-2015
Complete List of Authors:	Hailu, Solomon; CSIR-Central Leather Research Institute, Chemical Laboratory Nair, Balachandran; Central Leather Research Institute, Chemical Laboratory Redi-Abshiro, Mesfin; Addis Ababa University, Chemistry department Diaz, Isabel; ICP-CSIC, Instituto de Catalisis y Petroleoqu; Addis Ababa University, Chemistry department Aravindhan, Rathinam; Central Leather Research Institute, Tessema, Merid; Addis Ababa Univesristy, Chemistry Department
Subject area & keyword:	

Experimental and Computational Studies on Zeolite-Y Encapsulated Iron(III) and Nickel(II) Complexes Containing Mixed-ligand of 2,2'-bipyridine and 1,10-phenanthroline

Solomon Legese Hailu [1,2], Balachandran Unni Nair [1,*], Mesfin Redi-Abshiro [2], Rathinam Aravindhan [1], Isabel Diaz [2,3], Merid Tessema [2]

[1] Chemical Laboratory, CSIR-Central Leather Research Institute, Adyar, Chennai 600 020, India

[2] Department of Chemistry, Addis Ababa University, P.O. Box 1176, Addis Ababa, Ethiopia

[3] Instituto de Catálisis y Petroleoquímica, ICP-CSIC, C/ Marie Curie 2, 28049 Cantoblanco, Madrid, Spain

∗ Corresponding author. Tel.: +91 44 2441 1630; fax: +91 44 2491 1589

E-mail address: bunninair@gmail.com

ABSTRACT

Mixed ligand complex of 2,2'-bipyridine and 1,10-phenanthroline with iron (III) and nickel (II) have been encapsulated into zeolite cage by the reaction of zeolite exchanged metal ion with flexible ligands. The synthesized catalyst has been characterized by X-ray powder diffraction, scanning electron microscopy, BET surface area and pore volume analysis, FT-IR spectroscopy, thermo-gravimetric analysis and elemental analysis. Density functional theory calculation has being carried out on both neat complexes as well as metal complexes encapsulated into NaY zeolite to investigate change in structural parameters, energies of the HOMO and LUMO, global hardness and softness of the two metal complexes upon encapsulation into zeolite. Experimental results confirm successful formation of mixed ligand complex of Fe(III) and Ni(II) inside the zeolite cage. Density functional theory calculations predict higher reactivity of the zeolite encapsulated metal complexes compared to respective metal complexes. The zeolite encapsulated Fe(III) and Ni(II) complexes are found to be catalytically active toward the oxidation of 2-phenyl phenol (OPP).

Keywords*:* Global softness; Koopmans theorem; Density Functional Theory; 2-phenyl phenol; Horvath-Kawazoe methods

1. Introduction

Over the past decade metal complexes have been extensively exploited as homogeneous catalysts for many reactions. Their high susceptibility to reaction condition, the difficulty of their separation from the product mixture, low thermal and chemical stabilities are the limitations of homogeneous catalyst.[1-3] To overcome this difficulty immobilization of the transition metal complexes in the voids of organic or inorganic supporting materials has been attempted. Among supporting materials used, zeolite and molecular sieves has gained considerable importance due to their unique characteristics of flexibility, ion exchange ability and stability.[4-7] Besides, the unique structure of the zeolite cage, the steric and electrostatic constraints imposed by the walls of the zeolite framework can influence the geometry of metal complex and hence change magnetic, electronic and redox properties of the encapsulated metal complex and this can lead to changes in the reactivity of encapsulated transition metal complex.[2,8-12] The cations in zeolite cage also play an important role in affecting the fate of transition metal complex in the cage, other than merely compensating the negative charge in zeolite framework.[13]

Immobilization of transition metal complexes in the zeolite cage can be achieved by either using flexible ligand or ship in a bottle (in-situ) method based on the size of the ligand. In both cases once the metal complex within zeolite cages is formed, it is too large to diffuse out.[7, 14-16] A theoretical investigation on the physical and chemical properties of complexes is important in order to study successful immobilization of metal complexes into zeolite supercage. Density functional theory (DFT) is a simple working tool in elucidating chemical reactivity as well as site selectivity of catalyst.[12, 15]

Synthesis of catalysts based on transition metal complexes of nitrogen containing heterocyclic compounds immobilized into zeolite supercage have attracted considerable attention in view of their potential for catalytic activity towards organic compounds. In this regards metal complexes containing diimine ligand such as 1,10-phenentroline and 2,2'-bipyridine have gained importance because of their versatile roles especially in catalysis.

However, all the encapsulation process reported so far contains only homo liganded compounds such as tris (2,2'-bipyridine) iron(II)$^{2+}$, tris (2,2'-bipyridine) ruthenium (II)$^{2+}$, tris(2,2'-bipyridine) cobalt(II)$^{2+}$ [17,18], bis (2,2'-bipyridine) nickel(II)$^{2+}$ [19], tris(2,2'-bipyridine) iron(II)$^{2+}$ [20,21], tris (1,10-phenanthroline) iron(II)$^{2+}$, tris (1,10-phenanthroline) cobalt(II)$^{2+}$, and tris(1,10-phenanthroline) zinc(II)$^{2+}$ [11] encapsulated into zeolite supercage. To the best of our knowledge, no study has been reported on the catalytic activity of zeolite-Y encapsulated mixed ligand complexes of

Fe(III) and Ni(II) containing both 2,2'-bipyridine (bipy) and 1,10-phenanthroline (Phen) coordinated to the metal ion. Therefore to exploit the combined effect of 1,10-phenantroline and 2,2'-bipyridine ligand on the catalytic property of the metal complex we have made an effort to synthesize zeolite encapsulated mixed ligand complexes of Fe(III) and Ni(II).

This communication describes the synthesis of zeolite encapsulated mixed ligand complexes and their catalytic activity towards oxidation organic pollutants in the tanning industry, i.e. 2-phenyl phenol (OPP). In the present study, besides the experimental work, quantum chemical calculations based on Density functional theory (DFT) methods have also been employed for both neat and encapsulated complexes to understand the impact of zeolite framework on the structure, electronic properties, and chemical reactivity of neat metal complexes.

2. Materials and Methods

2.1. Experimental

2.1.1. Chemicals and instruments

The zeolite Na-Y, 1,10-phenanthroline and 2,2'-bipyridine and were purchased from Sigma-Aldrich, India. The other chemicals were of AR quality. The X-ray powder diffractograms of neat zeolite and solid catalysts were recorded using Miniflux 11, Rigaku difractometer with Cu-Kα radiation (λ = 0.1548 nm). SEM images were taken using Quanta FEG 200-High Resolution Scanning Electron Microscope (HR-SEM). Surface area and pore volume of the neat zeolite and catalysts were determined by BET and HK method of nitrogen adsorption using an ASAP-2020, Micromeritics. FT-IR spectra of the neat zeolite, metal complexes and solid catalysts were recorded in the range of 400 - 4000 cm^{-1} using Perkin-Elmer FT-IR spectrophotometer in KBr methods. TGA analyses of neat zeolite, metal complexes and zeolite encapsulated metal complexes were recorded from room temperature to 800 ^{o}C at a heating rate of 10 ^{o}C/min in nitrogen atmosphere using TA instruments TGA Q50 thermal analyzer. After completely destroying the zeolitic framework with hot concentrated sulphuric acid and hydrofluoric acid, sodium, aluminium, iron and nickel metal ions were analyzed by Prodigy Xp high dispersion Inductive Coupled Plasma (ICP) Si content was determined by gravimetric methods. The CHN analysis was carried out using Vario MACRO cube elemental CHN analyzer.

2.1.2. Preparation of (2,2-bipy) (1,10-Phen) Iron(III) and Nickel(II) Complex

The two complexes were synthesized by reacting the respective metal salts with the ligands in 1:1:1 mole ratio, i.e. one mole of metal salt: one mole of 2,2'-bipyridine: one moles of 1,10-phenanthroline. A 2.0 mmol solution of 1,10-phenanthroline in 25 mL of ethanol was added drop wise to 2.0 mmol solution of respective metal salts in 10 mL of water while stirring magnetically at room temperature. In a drop wise mode 2 mmol 2,2'-bipyridine ethanolic solution was added in the above homogenous solution under stirring. The solution mixture was continuously stirred at room temperature for one more hour and allowed to stand for five days till it forms crystals.

2.1.3. Iron(III) and Nickel(II) Exchange Zeolites

The metal exchanged zeolite was prepared with little modification of the previously reported method.[3, 14] 3 g of respective metal salts i.e. ferric chloride and nickel(II) chloride, was dissolved in 250 mL of warm distilled water. To the solution 5 g of zeolite-Y was added under stirring. The reaction mixture was heated under reflux for 24 hr and cooled. Then the solid was filtered and washed thoroughly with hot distilled water several times till all the unfixed metal ions were removed from the surface of the zeolite. The washed solids were dried for 15 h at 150 ^{o}C in air oven.

2.1.4. Encapsulation of (2,2-bipy) (1,10-Phen) Iron(III) and Nickel(II) Complex in Na-Y Zeolite

Encapsulations of the complexes into the zeolite supercage were done using in situ or Ship-in-a-bottle method. 1 g of the corresponding metal exchanged zeolite and 1 mmol 1,10-phenanthroline was dissolved in 25 mL of ethanol and refluxed under constant stirring for 24 h. Subsequently the solution was cooled and the solid product formed was filtered. Then a solution of 1 mmol 2,2'-bipyridine in 25 mL ethanol was added to the solid product and refluxed under constant stirring for 24 h at constant temperature of 150 ^{o}C. Then the solution was kept for three consecutive days for proper formation of complexes in the zeolite supercage. Next the solid product was subjected to Soxhlet extraction for removing surface adsorbed ligands and metal complexes. The extraction was done with methanol, dichloromethane and diethyl ether till the washings were colorless. Finally, any uncomplexed metal ions, remaining in surface or inside the zeolite cage after complex formation, was removed by back exchanged process by stirring zeolite encapsulated metal complex with 0.01 M of NaCl solution for 3 h. Then the solid product was washed with hot water to remove the chloride ion and dried at 100 ^{o}C overnight.

2.2 Computational Method

All density functional theory (DFT) calculations were carried out using the DMol^3 program employed with generalized gradient approximation (GGA) in the Perdew-Burke-Ernzerh of (PBE) exchange functional and double numeric (DN) basis set. In the self-consistent field calculations, the electronic density convergence threshold was set to $1x10^{-6}$. Geometric optimization was performed with convergence thresholds of 10^{-5} Ha for the energy, $2x10^{-3}$ Ha/Å for the force, and 10^{-3} Å for the atomic displacements. We have performed all electronic structure calculations for neat $[Fe(bipy)(phen)Cl_2]^+$, $[Ni(bipy)(phen)Cl]^+$ and zeolite-Y encapsulated $[Fe(bipy)(phen)Cl_2]^+$ and $[Ni(bipy)(phen)Cl]^+$. Zeolite provides well-defined rigid and stable framework with cavities of various sizes and shapes, so that the encapsulation of transition metal complexes in these cavities allows us to vary their environment in a controlled manner. The supercage of zeolite Y was fixed its diameter is about 13.0 Å and its openings approximately 7.4 Å. Initially, the zeolite clusters were generated by taking 48 tetrahedral units (48T) of faujasite structure around the supercage, saturating them with hydrogen atoms and the framework of Si and O atoms of the clusters are held fixed at their crystallographic positions then all the terminal H atoms are optimized. The gas phase optimized complexes were encapsulated inside the supercage and the calculation was repeated. Based on the Koopmans theorem global hardness (η) value was calculated as follows $\eta = \frac{E_{LUMO} - E_{HOMO}}{2}$ (1)

Where: E_{LUMO} is the energy of the lowest unoccupied molecular orbital and E_{HOMO} is the energy of the highest occupied molecular orbital. The global softness (s) was calculated according to Parr et al. as follows [22] ;

$$s = \frac{1}{2\eta} \quad (2)$$

2.3. Studies on catalytic activity of synthesized catalyst

2.3.1. Catalytic activity studies (decomposition of H_2O_2)

The catalytic activities of zeolite encapsulated metal complexes were investigated for the decomposition of H_2O_2 at two different time intervals (1 and 2 h). An amount of 0.15 g of respective catalysts were added to 0.10 M solution of H_2O_2 in dynamic condition and the solution was kept on a universal shaker (80 rpm) for a period of 120 min. At the end of each reaction

time, catalyst was filtered and the partly decomposed H_2O_2 was diluted to 250 mL. Then 10 mL of this solution was titrated against standard $KMnO_4$ solution after addition of 20 mL of 2 M H_2SO_4 and 20 mL distilled water.[23]

2.3.2. Catalytic Oxidation of 2-Phenyl Phenol (OPP)

The oxidation of 2-Phenyl Phenol (OPP) was carried out in a batch reactor. In a 250 mL conical flask, 50 mL of 25 mg/L 2-Phenyl Phenol (OPP) solution was treated with 0.10 M H_2O_2 and 0.15 g of respective catalyst. The experiments were conducted at room temperature (29±2 ^oC) in dynamic condition on a universal shaker (80 rpm) for a period of 120 min. The reaction was monitored by taking aliquots of the sample at seven different reactions time (i.e. 10, 20, 40, 60, 80,100 and 120 min). After the samples had been taken from the reaction mixture, it was centrifuged and filtered then measured the absorbance of the filtrate at 287 nm using Shimadzu UV-1800 spectrophotometer.

3. Results and discussions

3.1. Experimental section

Since only 1:1 molar ratio of metal ion to ligand was used in the synthesis of the metal complex and the fact that 1,10-phenanthroline has high affinity for metal ions and it also possesses π-acceptor capability, in the first step of synthesis it forms simple metal-phen intermediate complexes. However, the final iron (III) or nickel (II) bipy-phen mixed liganded complexes were formed in the second step by addition of 2,2'-bipyridine ligand to the intermediate metal phenanthroline complex. When only phen or bipy was used as the ligand, simple complexes of Fe(III) and Ni(II) product were formed (see supporting information). To verify the formation of mixed ligand metal complexes the synthesized complexes were subjected ESI-MS. The ESI-MS spectrum of the Fe(III) complex and Ni(II) complexes are shown in Fig.S1a & Fig.S1b (Supporting information). The Fe(III) complex shows a base peak at m/z 461.408 which can be attributed to the cationic complex $[Fe(bipy)(phen)Cl_2]^+$. Similarly the ESI-MS spectrum of the Ni(II) complex shows major peak at m/z 429.435 which can be attributed to the cationic species $[Ni(bipy)(phen)Cl]^+$.

The zeolite-Y structure contains uniform sized pores and cages. The supercages have internal diameter of ~13.0 Å and are connected to each other by tunnels or "windows" of ~7.4 Å diameter.[17,18] Therefore, only active components with appropriate size and shape can be incorporated into this cage. The diameter of $[Fe(bipy)(phen)Cl_2]^+$ and $[Ni(bipy)(phen)Cl]^+$ is too large to effectively pass through the free aperture of zeolite supercage , but it is small enough to be confined in the larger cavities once it forms a complex in the cage. On the other hand, their easily flexibility nature of 2,2′-bipyridine and 1,10-phenanthroline ligand they can diffuse into zeolite and form complexes with previously exchanged metal ions inside the supercage using in-situ method. After metal to mixed ligand complex was formed inside the zeolite cage the catalyst was then purified by extensive Soxhlet extraction with methanol, dichloromethane and diethyl ether to remove unfixed or free ligand present on the surface and inside the supercages of zeolite. Similarly, any uncomplexed metal ions present in the zeolite lattice after purification was also removed with back exchange of encapsulated metal complexes by treating with 0.01 M NaCl solution.

Morphological and textural properties of materials

Fig. 1 shows the X-ray powder difractograms of neat zeolite-Y, iron(III) and nickel(II) catalyst. The diffraction pattern indicates that a well crystalline zeolite encapsulated catalysts have been

formed. Diffraction patterns of both zeolite encapsulated metal complexes are similar to that observed for the neat zeolite. The similarity of XRD pattern of all the samples suggests that the crystallinity of zeolite-Y has been preserved during encapsulation of respective metal complexes into zeolite cage. However, as shown in the Figure 1, a slight change in the peak intensity was observed around $2\theta < 20^{o}$, i.e. I_{220} at $2\theta = 10°$ and I_{311} at 12°, for both neat zeolite and metal catalyst.[11,12] The relative peak intensity for zeolite-Y is $I_{220}>I_{311,}$whereas, for zeolite encapsulated metal complexes, it is observed that, $I_{311}>I_{220}$. This change in relative intensities may be associated with redistribution of randomly coordinated metal cations in zeolite Y at sites II and I. Similar observation has been reported before[11,15] and the above observation may therefore be construed as evidence for the successful encapsulation of $[Fe(bipy)(phen)Cl_2]^+$ and $[Ni(bipy)(phen)Cl]^+$ complex within the supercage of zeolite Y.

After encapsulation of the respective metal complexes into zeolite supercage the solid catalyst was purified by extensive Soxhlet extraction with organic solvents to remove unreacted ligand and/or surface adsorbed complexes. SEM morphology of the metal catalysts before and after Soxhlet extraction is depicted in Fig.2. In the SEM image (Fig. 2a,c) taken before purification there are no defined particle boundaries owing to the metal complexes deposited on the external surface of zeolite. Whereas the SEM image (Fig. 2b,d) of the all catalysts after solvent extraction show particle boundaries indicating that surface adsorbed complexes are not present in this case. This revels the efficiency of the Soxhlet extraction procedure to effectively remove extraneous complexes, leading to well defined encapsulation in the zeolite cavity. Moreover, encapsulation of respective metal complexes into zeolite supercage does not affect the crystal structure of the parent zeolite.

The Surface area and pore volume studies of neat zeolite (NaY), $[Fe(bipy)(phen)Cl_2]^+$-Y and $[Ni(bipy)(phen)Cl]^+$-Y was conducted using Brunauer-Emmett-Teller (BET) and Horvath-Kawazoe methods (HK) respectively and the results are shown in Fig.3. The two catalysts and neat zeolite show typical type-I hysteresis loops in their N_2 sorption isotherms and according to IUPAC and Brunauer et al. classification of porous material they are characteristic of micro porous materials.[24,25] This is also indicates that the characteristic micro porous structure of NaY is not damaged during the encapsulation of metal complexes into zeolite supercage. The surface area of NaY has the values of 634 m^2/g. However, after encapsulation of respective metal mixed ligand complexes into the zeolite cage the surface area is reduced to 519 m^2/g and 548 m^2/g for

$[Fe(bipy)(phen)Cl_2]^+$-Y and $[Ni(bipy)(phen)Cl]^+$-Y catalyst, respectively. The pore volume of NaY (0.227 cm^3/g) is also reduced to 0.139 cm^3/g and 0.157 cm^3/g for $[Fe(bipy)(phen)Cl_2]^+$-Y and $[Ni(bipy)(phen)Cl]^+$-Y respectively, is primarily due to the presence of respective metal complexes in the pores of zeolite. This clearly suggests that the metal-(bipy)(phen) complex was encapsulated in the cavities of zeolite.

Spectroscopic characterization

The FT-IR spectra of NaY as well as that of $[Fe(bipy)(phen)Cl_2]^+$ and $[Ni(bipy)(phen)Cl]^+$ complex encapsulated into zeolite cage are provided in Fig.4. It can be seen that IR spectra of the two catalysts are dominated by the IR bands of zeolite. The broad bands in the regions 3450 and 1650 cm^{-1} are due to asymmetric stretching and bending mode of water molecules or surface hydroxylic groups, respectively.[3,26] FTIR spectra of neat zeolite-Y show strong zeolite lattice bands in the range of 450-1100 cm^{-1}.[1] The strong and broad bands in the region 1010-1030 cm^{-1} could be attributed to the asymmetric stretching vibrations of $(Si/Al)O_4$ units.[14,26] The parent zeolite shows characteristic bands at 455, 559, 663, and 975 cm^{-1} that are attributed to T-O bending mode, symmetric and asymmetric stretching.[3,14] Those neat zeolite bands are also observed with little band shift upon introduction of the metal complexes into the zeolite supercage. This again suggests that the metal complex encapsulated catalysts retain the zeolite framework. The specific IR bands of the two encapsulated metal complexes are very weak because of their low concentration in the zeolite cage. The neat iron(III), and nickel(II) complexes show -C=C- stretching and -C-H- bending between 1310-1585 cm^{-1} and 720-850 cm^{-1}, respectively. Similar IR bands are also observed in the case of all encapsulated metal complexes with a little shift in the position of the bands. The band observed at 1516 and 1425 cm^{-1} in the case of the metal complexes is observed at 1522 cm^{-1} and 1422 cm^{-1} for iron(III) catalyst,1512 cm^{-1} and 1426 cm^{-1} for nickel(II) catalyst. Thus, the IR spectra of the catalysts indicate the formation of respective metal bipy-phen complex inside the cavity of zeolite framework.

The thermogravimetric (TGA) and derivative thermogravimetry (DTG) patterns of NaY, $[Fe(bipy)(phen)Cl_2]^+$ and $[Ni(bipy)(phen)Cl]^+$ complexes and zeolite encapsulated $[Fe(bipy)(phen)Cl_2]^+$ and $[Ni(bipy)(phen)Cl]^+$ complexes are displayed in Fig. 5a and Fig. 5b. The two metal complexes exhibit three weight loss steps (Fig. 5a) and on the basis of weight

changes, the first weight loss step in both neat complexes corresponds to the loss of water molecule as an exothermic phenomenon. The second weight loss may be related to the loss of Cl_2 molecule coordinated to the central metal ions. In the last stage there is a sharp decomposition with highest percentage of weight change at 364 °C for the iron(III) complex and at 417 °C for the nickel(II) complex and this weight loss is associated to the loss of organic moieties of the complexes. Though, the respective zeolite encapsulated metal complexes show only two weight loss stages. The first weight loss in the temperature range of 0-150 ^{o}C is mainly to desorption of physically adsorbed and possibly chemically bonded water molecules. The second stage weight loss covering the wide temperature range (150-800 ^{o}C) is predominantly the decomposition of organic part of the catalyst and chlorine molecules coordinated to the central metal ions. Fig. 5b TGA-DTG graph shows there is sharp weight change in the exothermic mode at 440 °C and 450 °C for $[Fe(bipy)(phen)Cl_2]^+$-Y and $[Ni(bipy)(phen)Cl]^+$-Y catalyst respectively, is attributed to loss of biy-phen mixed ligands. The corresponding encapsulated complex the weight loss extend up to 500 °C, which indicates that the thermal stability of the metal complex is greatly enhanced once they encapsulated into a highly thermal resistant aluminosilicate frame work of zeolite Y. The loss of total organic component in the case of $[Fe(bipy)(phen)Cl_2]^+$-Y and $[Ni(bipy)(phen)Cl]^+$-Y upon heating upto 800 °C is nearly consistent with the data obtained from CHN analysis (Table 1). Small weight difference observed is due to decomposition of chloride ion coordinated to the metal ions.

Quantification

Table 2 shows the result of quantitative analysis of neat zeolite, neat metal complex and zeolite encapsulated metal complexes in molar ratio. The Si/Al ratio of neat zeolite-Y, zeolite encapsulated iron(III) and nickel(II) complex is 2.46, 2.44 and 2.45 respectively. This revels that there is no dealumination during encapsulation of respective metal complexes into zeolite supercage hence the zeolite framework does not affected because of encapsulation process. As observed in the Table 2, the metal, carbon and nitrogen value for the neat metal complexes and encapsulated metal complexes has almost similar carbon to nitrogen ratio with respect to the theoretical value of the respective metal complexes. This is a good evidence for the successful formation exclusively mixed-ligand metal complexes of $[Fe(bipy)(phen)Cl_2]^+$ and $[Ni(bipy)(phen)Cl]^+$ in zeolite supercage with complexation of four nitrogen ligands with iron(III) and nickel(II) central metal ion. However, minute traces of free metal ions are present in

the zeolite cage even after back exchange processes were applied with 0.01 N NaCl. The presence of trace amount of non exchangeable free metal ions may be attributed to the shielding by the guest molecules (metal complex) or some of the sites in the zeolite lattice might be blocked by the encapsulated metal complexes for NaCl solution to access the free metal ion in back exchanged process.[27] It has been also reported that traces of uncomplexed metal ions are not causing any interference in the behavior of the zeolite encapsulated metal complexes.[9, 28]

Theoretical Calculation

The geometrical parameters obtained from PBE /DN level calculations for the neat and encapsulated metal complexes are depicted in Table 3. The geometrical parameters (such as bond length, bond angles and dihedral angle) of $[Fe(bipy)(phen)Cl_2]^+$ and $[Ni(bipy)(phen)Cl]^+$ have been compared with that of zeolite encapsulated $[Fe(bipy)(phen)Cl_2]^+$ and $[Ni(bipy)(phen)Cl]^+$ and are found to be in good agreement. The average bond length differences observed between neat metal complex and zeolite encapsulated metal complexes after optimization is 0.081 and 0.037 Å for $[Fe(bipy)(phen)Cl_2]^+$ and $[Ni(bipy)(phen)Cl]^+$ respectively. Similarly bond angle difference of 2.862 and 5.564 degree has been observed for $[Fe(bipy)(phen)Cl_2]^+$ and $[Ni(bipy)(phen)Cl]^+$ respectively. This revels that, once the metal complex was encapsulated into the zeolite-Y cage, bond angle between the respective metal and ligand molecules slightly change in comparison to those of the corresponding neat metal complexes. The most prominent differences are observed in the values of the bond angle and dihedral angles around the metal ion. The change in bond angle and dihedral angle of the metal complexes on encapsulation maybe attributed to the influence of zeolite framework. It has previously been reported that Si-O bonds in zeolites have solely covalent character.[12] Therefore the structural and electronic properties of the encapsulated metal complexes are expected to be influenced by the electron-electron repulsions between the metal complex and the nearby partially delocalized electrons in the zeolite supercage.

Fig.6 shows the highest occupied molecular orbital (HOMO) and the lowest unoccupied molecular orbital (LUMO) for the neat complexes and zeolite encapsulated metal complexes and their energies are given in Table 4. We have performed spin-unrestricted calculations on all the systems and the energies of HOMO and LUMO orbitals that correspond to the spin-up and spin-down state were found to be same in both neat and encapsulated system of iron (III) and nickel

(II) mixed ligand complexes. It is observed from Table 4 that the individual HOMO-LUMO energy of the metal complexes increases upon encapsulation into zeolite, indicating that the complexes are destabilized upon encapsulation. Moreover, the HOMO-LUMO gap (ΔE_{H-L}) of $[Fe(bipy)(phen)Cl_2]^+$ and $[Ni(bipy)(phen)Cl]^+$ has been found to decrease on encapsulation (Fig.S2). This indicates that transfer of electrons from the prepared catalysts is much more viable than neat complexes. The change in the energies of the HOMO-LUMO orbital upon encapsulation of $[Fe(bipy)(phen)Cl_2]^+$ and $[Ni(bipy)(phen)Cl]^+$ may be either due to the effect of the counter ion in zeolite Y or due to the steric constraint generated by the zeolite supercage. A metal complex confined inside the zeolite is subjected to coulombic effect. This coulombic effect is produced by the charge distribution along the framework because of the partial ionic character of the zeolite lattice. This charge distribution generates a strong coulombic field in the cavities, which might alter the energy level of the transition-metal complexes.[11, 12, 29]

Applying the Koopmans' theorem, global hardness (η) and softness (s) values of the neat and encapsulated complexes have been calculated. It can be seen from Table 4 that the global hardness values of $[Fe(bipy)(phen)Cl_2]^+$ and $[Ni(bipy)(phen)Cl]^+$ decrease on encapsulation into the zeolite cavities. On the other hand, the softness values of the metal complexes increase on encapsulation. According to the maximum hardness principle (MHP) and the minimum polarizability principle (MPP), (the hardness measures the stability of structure and the polarizablity (softness) measures reactivity), the most stable structure has maximum hardness and the less reactive species has minimum softness value. Hence, it is clear that the complexes $[Fe(bipy)(phen)Cl_2]^+$ and $[Ni(bipy)(phen)Cl]^+$ are destabilized and become more reactive on encapsulation compared to free metal complexes.

3.3. Application of synthesized catalyst for oxidation of OPP

The potential catalytic ability of synthesized catalyst was investigated over the decomposition of hydrogen peroxide through time. Unlike in the conventional Fenton system, methanol was employed as a reaction medium and the percentage decomposition of hydrogen peroxide was measured at two different reaction times (1 h & 2 h). The results show that the decomposition of hydrogen peroxide after 1 h is relatively slow for both iron (6.89%) and nickel (4.63%) based heterogeneous catalyst. However, after 2 h contact time the decomposition rate of hydrogen peroxide became higher for iron (22.75%) than nickel (19.47%) catalyst. Thus, these results indicate that $[Fe(bipy)(phen)Cl_2]^+$-Y and $[Ni(bipy)(phen)Cl]^+$-Y require a relatively longer contact time to attain the maximum equilibrium for generation of hydroxyl radicals.[1, 28,30]

To study the role of catalyst and hydrogen peroxide in degradation of OPP through specific time, two independent experiments have been carried out. In one experiment, hydrogen peroxide was used without any catalyst, in the other set of experiments; hydrogen peroxide together with iron(III) and nickel(II) catalysts was employed with initial OPP concentration of 25 mg/L.

It could be observed from the Fig. 7a that the residual concentration of OPP is 5.46 mg/L and 7.14 mg/L for experiments carried out in the presence of iron(III) and nickel(II) catalyst, respectively. It is known that encapsulation of metal complexes in zeolites can result in unusual oxidation states/electronic configurations and a unique chemical property of zeolite encapsulated metal complexes and this enables the formation of hydroxyl radicals (•OH) from hydrogen peroxide. Even though hydrogen peroxide is a well known oxidizing agent with high mobility in the pores of zeolite systems, the experiment conducted with hydrogen peroxide alone did not result in a significant oxidation of OPP. The residual concentration of OPP was 19.34 mg/L after 120 min reaction time. This observation clearly indicate that to attain maximum oxidation of OPP, along with enhancement in the rate of the reaction, the presence of $[Fe(bipy)(phen)Cl_2]^+$-Y and $[Ni(bipy)(phen)Cl]^+$-Y catalyst has a vital role. Alteration of redox potential of metal complexes by the partially delocalized electron cloud of zeolite supercage is responsible for increasing the catalytic performance of both catalysts. However, the better catalytic performance exhibited by the iron(III) catalyst than nickel(II) based catalyst may be attributed to higher

oxidizing capability of the Fe(III)/Fe(II) than Ni(II)/Ni(I). It is worthwhile to compare the catalytic efficiency of the zeolite encapsulated mixed ligand complexes with that of zeolite encapsulated Fe(III) and Ni(II) complexes of individual ligands (phen and bipy). The residual concentration of OPP when $Fe(phen)_2Cl_2^+$, $Ni(phen)_2Cl^+$, $Fe(bipy)_2Cl_2^+$ and $Ni(bipy)_2Cl_2^+$ were used as catalyst under identical conditions were 8.19 mg/L, 8.75 mg/L, 10.81 mg/L and 11.66 mg/L respectively (see supporting information). Hence, it is clear that the mixed ligand complexes of Fe(III) and Ni(II) are more efficient catalysts for the oxidation of OPP than the individual complexes of phen or bipy.

In the other set of experiments the efficiency of zeolite based heterogeneous catalyst was compared with its corresponding homogeneous catalyst by taking the same amount of active metal complexes and the reaction processes were operated at same reaction conditions. As shown in Fig. 7a & Fig. 7b**,** that the residual concentration of OPP left after 120 min oxidation time using homogeneous catalyst is 8.81 mg/L and 10.08 mg/L for iron and nickel catalyst, respectively. Thus, the metal catalysts in heterogeneous phase have better overall catalytic efficiency than its homogenous counterparts. However, the rate in the heterogeneous phase is lower than that of observed in the homogeneous phase, which may be due to reduced accessibility between the catalyst active site of $[Fe(bipy)(phen)Cl_2]^+$-Y and $[Ni(bipy)(phen)Cl]^+$-Y catalyst and H_2O_2 as the complex is occluded in the zeolite channels. Therefore, the observed efficient performance of heterogeneous catalyst over homogeneous catalyst is on account of steric and electrostatic constraints imposed by the walls of the zeolite framework.[11, 12] Moreover, heterogeneous catalyst system remains active after successive oxidation of OPP in the first run.

The important point concerning heterogeneous catalysis is the reusability of the catalyst, which is very vital in the application of a new catalytic system. To test this, a series of three consecutive runs of reaction were carried out for each catalyst. The encapsulated catalyst separated out from the reaction mixture then washed with organic solvent, dried and subjected to further catalytic reaction under the similar conditions. The residual concentration obtained after the first, second and third cycle of iron(III) and nickel(II) catalyst is about 5.52, 5.71, 5.78 mg/L and 7.39, 7.55, 7.67 mg/L respectively. The obtained result further indicates that the synthesized catalyst could be reused more than three times without losing its efficiency over the catalytic process. This fact demonstrates that the metal complex once encapsulated in the supercages of

zeolite affords reactive centers, and the porous support prevents the complex from leaching and decomposition under reaction conditions and makes it recoverable.

4. Conclusions

NaY zeolite encapsulated Fe(III) and Ni(II) complexes of 2,2'-bipyridine and 1,10-phenanthroline mixed ligand were prepared using a ship-in-a-bottle method. The characterization result obtained by XRD, SEM, BET, TGA, FT-IR and elemental analysis confirms the encapsulation of the metal complexes in the supercages of the NaY zeolite. The computational part of studies for neat Fe(III) and Ni(II) complexes as well as zeolite encapsulated metal complexes also support the successful formation of respective metal complexes in the zeolite cage. HOMO-LUMO energies, global hardness and softness value of the metal complexes change once the metal complexes are encapsulated into the zeolite cage. The change in bond angle and dihedral angle of the metal complexes on encapsulation maybe attributed to the steric constraints of zeolite framework. The synthesized zeolite-encapsulated metal complexes were active catalysts for the decomposition of hydrogen peroxide and for the oxidation of OPP with good efficiency. The reusability test on the catalyst also confirms that zeolite encapsulated metal complex could be used more than three times without losing their catalytic efficiency.

Acknowledgements

Solomon Legese Hailu sincerely thanks the Leather Industry Development Institute (LIDI), Government of Ethiopia, Addis Ababa, for full financial support for his PhD studies under Twinning Program between Leather Industry Development Institute (LIDI), Addis Ababa University (AAU) and CSIR-Central Leather Research Institute (CLRI). ID acknowledges CSIC, Spain for the research leave at AAU.

References

1 M.R. Maurya, S.J.J. Titinchi, S. Chand, *J. Mol. Catal. A: Chem*., 2003, **201,** 119-130.

2 P. Chen, B. Fan, M. Song, C. Jin, J. Ma, R. Li, *Catal. Commun*., 2006, **7**, 969-973.

3 M.R. Maurya, S.J.J. Titinchi, S. Chand, I.M. Mishra, *J. Mol. Catal. A: Chem*.,2002, **180**, 201-209.

4 M.R. Maurya, S.J.J. Titinchi, S. Chand, *J. Mol. Catal. A: Chem*.,2004, **214**, 257-264.

5 R. Abraham, K.K.M. Yusuff, *J. Mol. Catal. A: Chem*.,2003, **198**,175-183.

6 C. Jin, W. Fan, Y. Jia, B. Fan, J. Ma, R. Li, *J. Mol. Catal. A: Chem*.,2006, **249**, 23-30.

7 S.M. Drechsel, R.C.K. Kaminski, S. Nakagaki, F. Wypych, *J. Colloid Interface Sci*., 2004, **27**,138-145.

8 M. Salavati-Niasari, *J. Mol. Catal. A: Chem*.,2006, **245**, 192-199.

9 K.K. Bania, G.V. Karunakar, K. Goutham, R.C. Deka, *J. Inorg. Chem.,2013*, **5**2, 8017-8029.

10 M. Jafarian, M. Rashvand avei, M. Khakali, F. Gobal, S. Rayati, M.G. Mahjani, *J.Phys. Chem. C*, 2012, **116**, 18518-18532.

11 K.K. Bania, R.C. Deka, *J. Phys. Chem.* C,2012, **116**,14295-14310.

12 R. Ganesan, B. Viswanathan, *J. Mol. Catal. A: Chem*.,2004, **223**, 21-29.

13 R. Grommen, P. Manikandan, Y. Gao, T. Shane, J.J. Shane, R.A. Schoonheydt, B.M. Weckhuysen, D. Goldfarb, *J. Am. Chem. Soc*.,2000,**122**,11488-11496.

14 T.M. Salama, A.H. Ahmed, Z.M. El-Bahy, *J.Micropor. Mesopor.Mater*., 2006, **89**, 251-259.

15 K.K. Bania, D. Bharali, B. Viswanathan, R.C. Deka, *J. Inorg. Chem*., 2012, **51**, 1657-1674.

16 A. Domenech, B. Ferrer, V. Fornes, H. García, A. Leyva, *Tetrahedron*, 2005, **61,** 791-796.

17 M.A. Coutant, T. Le, N. Castagnola, P.K. Dutta, *J. Phys. Chem. B*, 2000, **104**, 10783-10788.

18 G. Sewell, R.J. Forster, T.E. Keyes, *J. Phys. Chem. A*,2008, **112**, 880-888.

19 R. Zăvoianu, C. Nenu, E. Angelescu, *Catal. Commun*.,2005, **6**, 415-420.

20 R. Vijayalakshmi, S.K. Kulshreshtha, *J. Micropor. Mesopor. Mater*., 2008, **111**, 449-454.

21 K. Mori, K. Kagohara, H. Yamashita, *J. Phys. Chem. C*,2008, **112**, 2593-2600.

22 R.G. Parr, L.v. Szentpály, S. Liu, *J. Am. Chem. Soc*.,1999, **121**, 1922-1924.

23 J. Bassett, R.C. Denney, G.H. Jeffery, J. Menhdham, Vogel's textbook of quantitative chemical analysis, Longman Scientific and Technical, London, 5th edn., 1989, pp. 372-373

23 K.S.W.Sing, D.H.Everest, R.A.W.Haul, L.Moscou, R.A.Pierotti, J.Rouquerol and T.Siemieniewska, *Pure & appl.chem*., 1985,**57**, 603-619

25 S. Brunauer, L.S. Deming, W.E. Deming, E. Teller, *J. Am. Chem. Soc*., 1940,**62**, 19401723-1732.

26 R. Ganesan, B. Viswanathan, *J. Phys. Chem. B*, 2004,**108**, 7102-7114.

27 Salavati-Niasari M , Salimi Z , Bazarganipour M , Davar F, *Inorg. Chim. Acta*.,2009, **362**, 3715-3724

28 Xavier K, Chacko J, Mohammed Yusuff K, *Applied Catal. A: General*, 2004, **258**, 251-259

29 S. Wannakao, P. Khongpracha, J. Limtrakul, *J. Phys. Chem. A*, 2011,**115**, 12486-12492.

30 N.N. Fathima, R. Aravindhan, J. R. Rao, B. U. Nair, *Chemosphere*, 2008,**70**, 1146–1151

Figure caption

Fig.1. XRD pattern of (a) NaY (b) $[Fe(bipy)(phen)Cl_2]^+$-Y and (c) $[Ni(bipy)(phen)Cl]^+$-Y

Fig.2. The SE micrographs of (a) $[Fe(bipy)(phen)Cl_2]^+$-Y before Soxhlet extraction (b) $[Fe(bipy)(phen)Cl_2]^+$-Y after Soxhlet extraction (c) $[Ni(bipy)(phen)Cl]^+$-Y before Soxhlet extraction (d) $[Ni(bipy)(phen)Cl]^+$-Y after Soxhlet extraction

Fig.3. N_2 sorption isotherms plot for NaY, $[Fe(bipy)(phen)Cl_2]^+$-Y & $[Ni(bipy)(phen)Cl]^+$-Y

Fig.4. FT-IR spectra of (a) NaY (b) $[Fe(bipy)(phen)Cl_2]^+$-Y & (c) $[Ni(bipy)(phen)Cl]^+$-Y

Fig.5. Thermogravimetric analysis (TGA) and derivative thermogravimetry (DTG) results for (a) $[Fe(bipy)(phen)Cl_2]^+$ & $[Ni(bipy)(phen)Cl]^+$ (b) NaY,$[Fe(bipy)(phen)Cl_2]^+$-Y & $[Ni(bipy)(phen)Cl]^+$-Y

Fig.6. Schematic representation of the HOMO and LUMO level of the neat and encapsulated complexes Fe(III) and Ni(II) complexes of 1,10-phenanthroline and 2,2'-bipyridine ligands

Fig.7. Oxidation of OPP in (a) heterogeneous catalyst and (b) homogeneous catalyst

Table caption

Table 1 Results of thermogravimetric analysis and CHN analysis for the catalyst sample

Table 2 Chemical composition of neat zeolite, neat metal complexes and metal catalyst

Table 3 Bond distances (in Å), bond angles (in degree) and dihedral angle (in degree) of the optimized neat complexes and zeolite encapsulated metal complexes, (M = Fe (III) and Ni (II))

Table 4 Calculated Energy of HOMO and LUMO (in eV), HOMO-LUMO gap (ΔE, in eV), Global Hardness (η, in ev) and Global Softness (S, in eV)

Figure caption

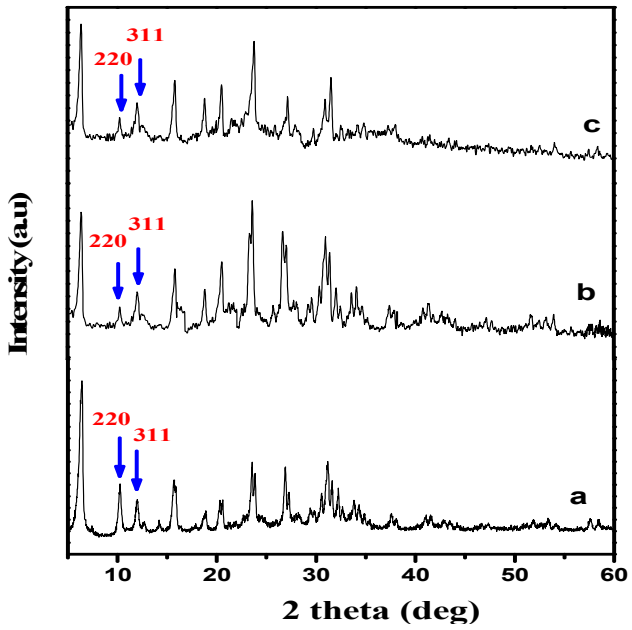

Fig.1. XRD pattern of (a) NaY (b) $[Fe(bipy)(phen)Cl_2]^+$-Y and (c) $[Ni(bipy)(phen)Cl]^+$-Y

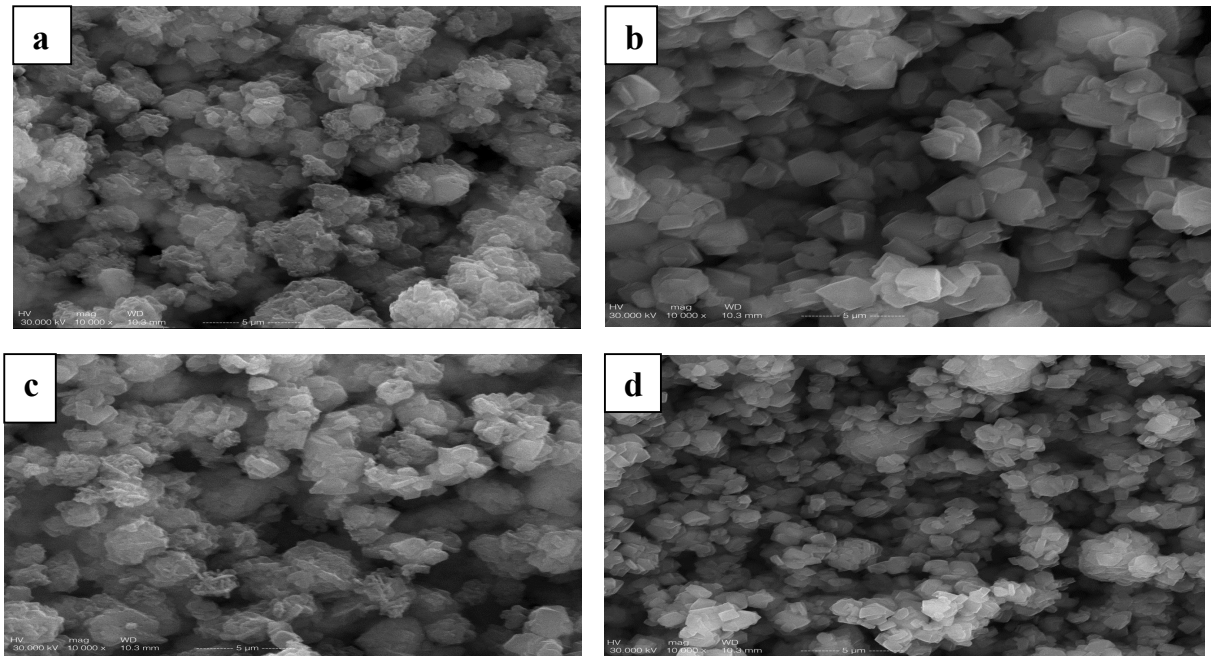

Fig.2. The SE micrographs of (a) $[Fe(bipy)(phen)Cl_2]^+$-Y before Soxhlet extraction (b) $[Fe(bipy)(phen)Cl_2]^+$-Y after Soxhlet extraction (c) $[Ni(bipy)(phen)Cl]^+$-Y before Soxhlet extraction (d) $[Ni(bipy)(phen)Cl]^+$-Y after Soxhlet extraction

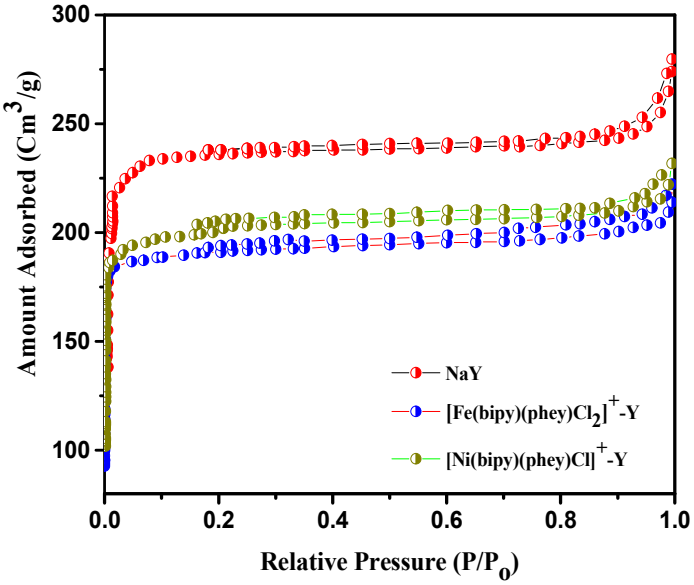

Fig.3. N_2 sorption isotherms plot for NaY, $[Fe(bipy)(phen)Cl_2]^+$-Y & $[Ni(bipy)(phen)Cl]^+$-Y

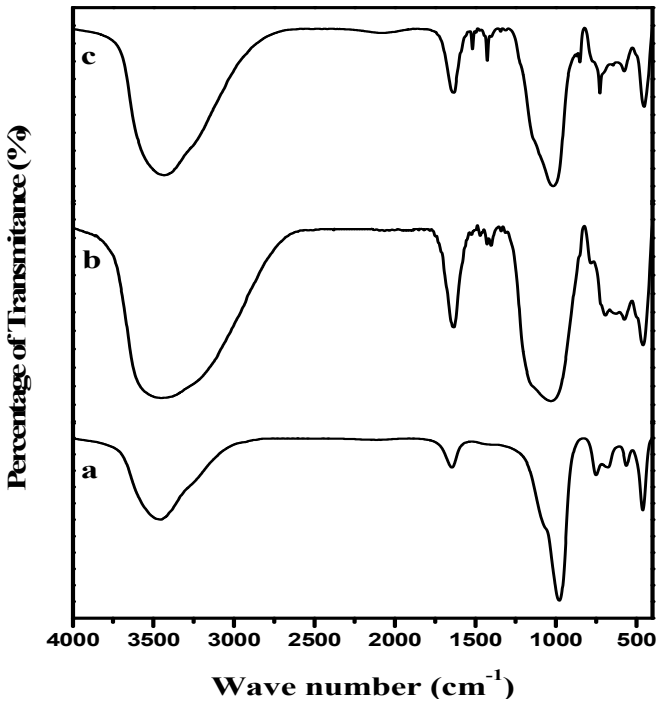

Fig.4. FT-IR spectra of (a) NaY (b) $[Fe(bipy)(phen)Cl_2]^+$-Y & (c) $[Ni(bipy)(phen)Cl]^+$-Y

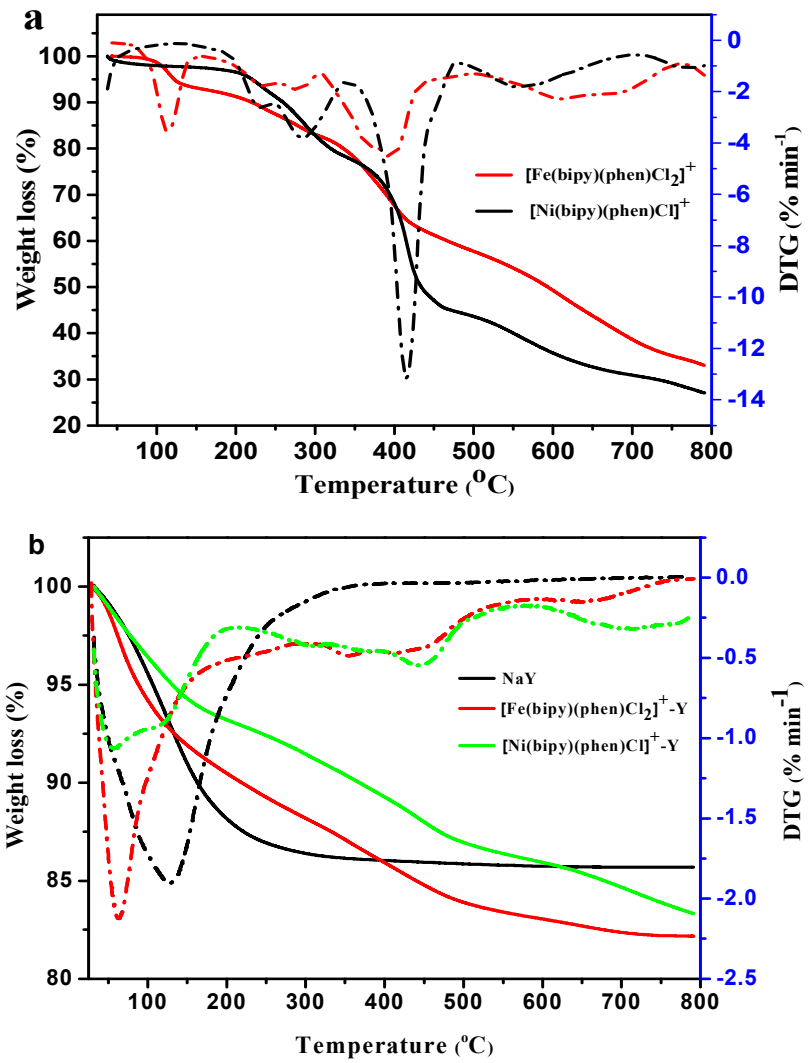

Fig.5. Thermogravimetric analysis (TGA) and derivative thermogravimetry (DTG) results for (a) $[Fe(bipy)(phen)Cl_2]^+$ & $[Ni(bipy)(phen)Cl]^+$ (b) NaY, $[Fe(bipy)(phen)Cl_2]^+$-Y & $[Ni(bipy)(phen)Cl]^+$-Y

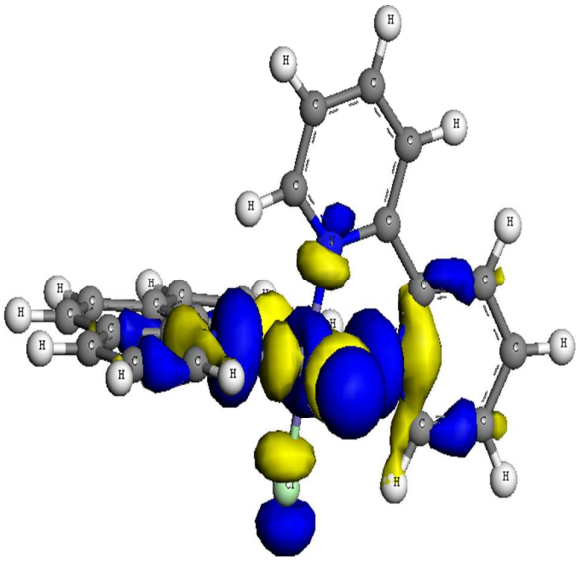

HOMO($[Fe(bipy)(phen)Cl_2]^+$)

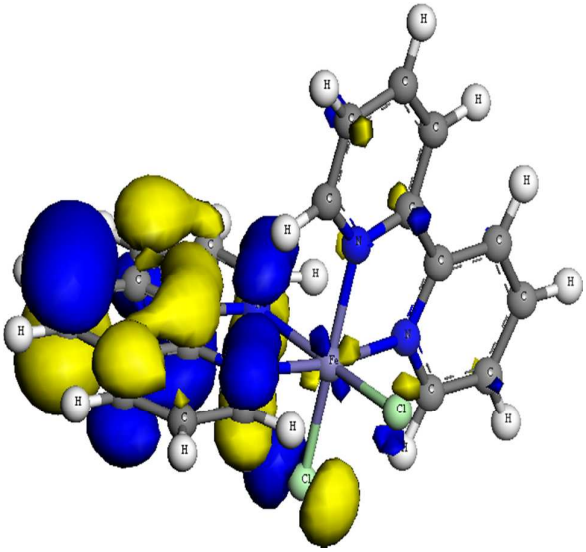

LUMO($[Fe(bipy)(phen)Cl_2]^+$)

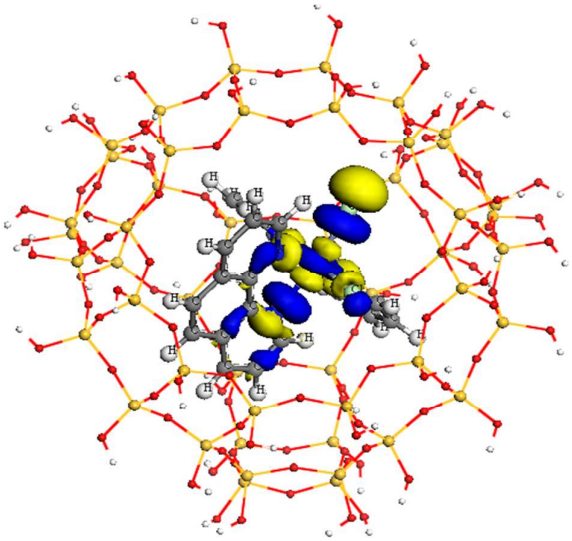

HOMO($[Fe(bipy)(phen)Cl_2]^+$-Y)

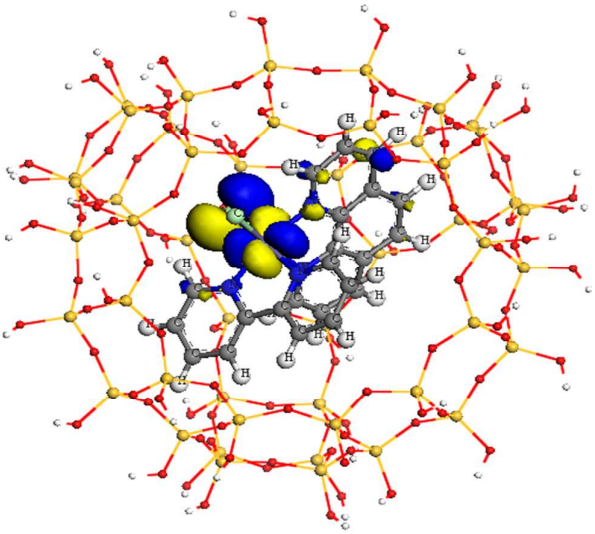

LUMO ($[Fe(bipy)(phen)Cl_2]^+$-Y)

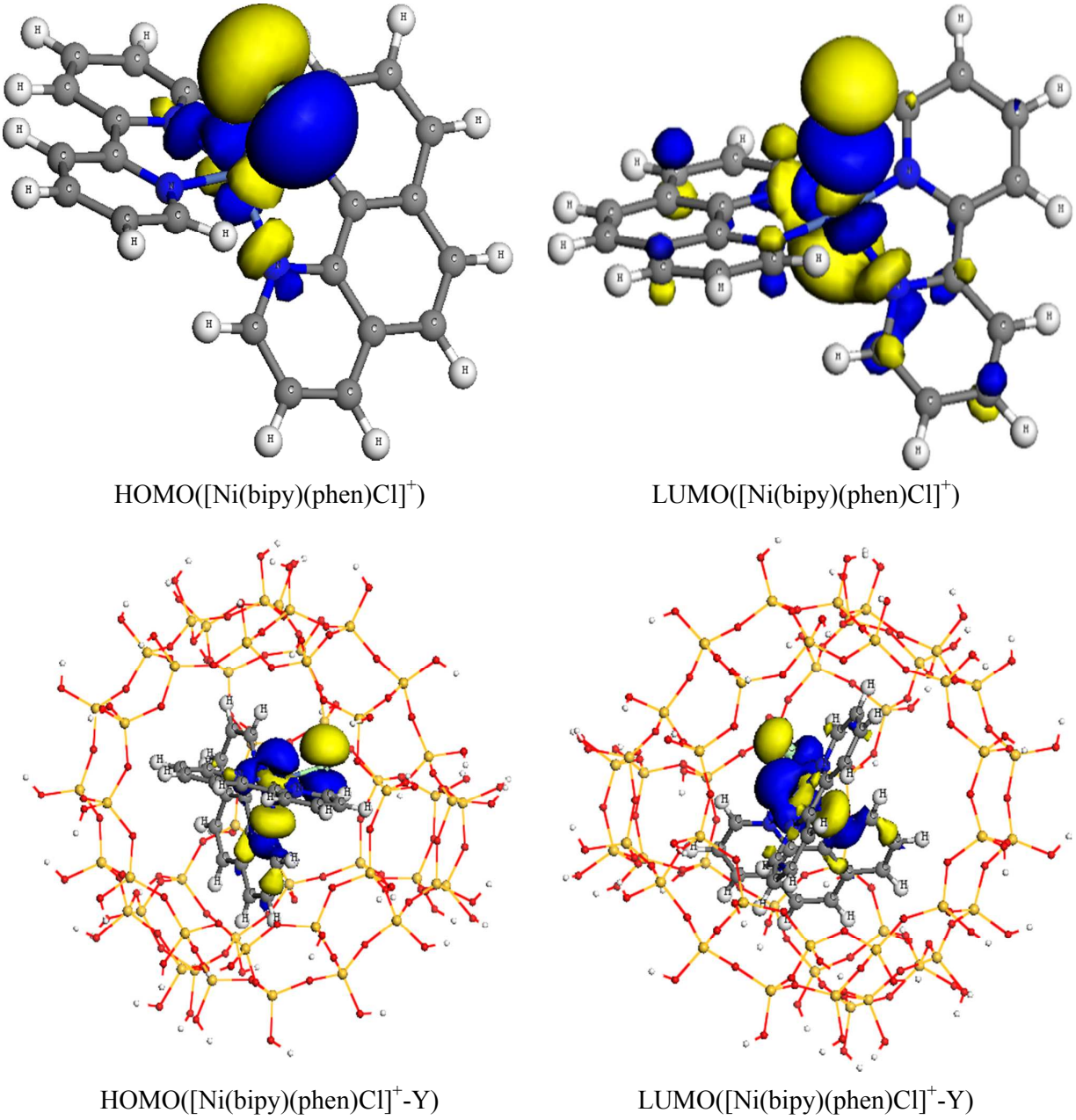

Fig.6. Schematic representation of the HOMO and LUMO level of the neat and encapsulated complexes Fe(III) and Ni(II) complexes of 1,10-phenanthroline and 2,2'-bipyridine ligands

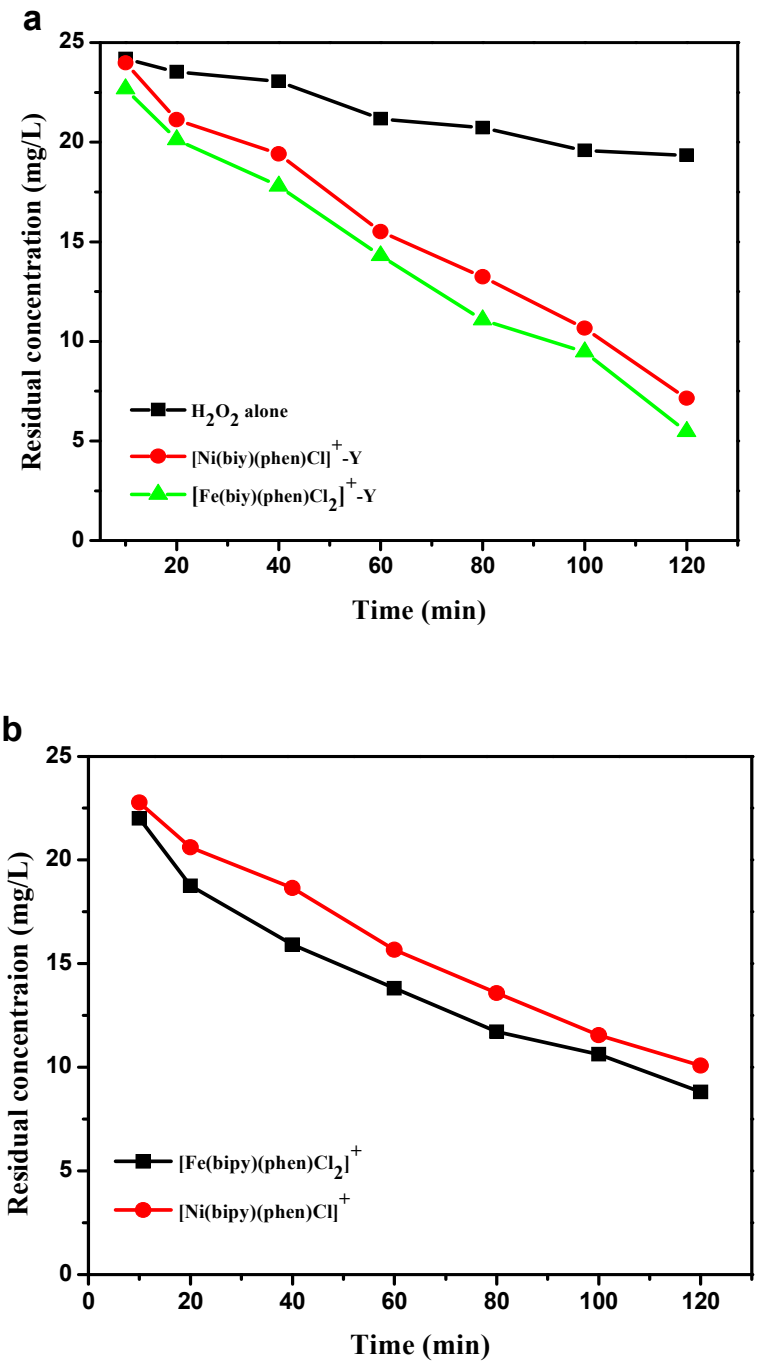

Fig.7. Oxidation of OPP in (a) heterogeneous catalyst and (b) homogeneous catalyst

Table caption

Table 1

Results of thermogravimetric analysis and CHN analysis for the catalyst sample

Sample	Temperature (^oC)	Weight loss (%)	Type of loss	Total CHN weight (%)
$[Fe(bipy)(phen)Cl_2]^+$-Y	0-150	7.93	Water desorption	-
	150-800	11.54	Complexes decomposition	10.52
$[Ni(bipy)(phen)Cl]^+$-Y	0-150	5.71	Water desorption	-
	150-800	10.85	Complexes decomposition	9.75

Table 2

Chemical composition (molar ratio) of neat zeolite, neat metal complexes and metal catalyst

Sample	Metal %	Si %	Al %	Si/Al	Na %	C %	N %	C/N
$[Fe(bipy)(phen)Cl_2]^+$	0.22 (0.21)[a]	-	-	-	-	4.75 (4.73)[a]	0.87 (0.86)[a]	5.46 (5.50)[a]
$[Ni(bipy)(phen)Cl]^+$	0.24 (0.23)[a]	-	-	-	-	5.12 (5.09)[a]	0.93 (0.92)[a]	5.51 (5.53)[a]
Zeolite-Y	-	0.79	0.32	2.46	0.32	-	-	-
$[Fe(bipy)(phen)Cl_2]^+$-Y	0.03	0.78	0.32	2.43	0.24	0.67	0.12	5.58
$[Ni(bipy)(phen)Cl]^+$-Y	0.03	0.76	0.31	2.45	0.23	0.62	0.11	5.63

- [a] is theoretical value

Table 3

Bond distances (in Å), bond angles (in degree) and dihedral angle (in degree) of the optimized neat complexes and zeolite encapsulated metal complexes, (M = Fe (III) and Ni (II))

	$[Fe(bipy)(phen)Cl_2]^+$	$[Fe(bipy)(phen)Cl_2]^+$-Y	$[Ni(bipy)(phen)Cl]^+$	$[Ni(bipy)(phen)Cl]^+$-Y
		Bond length		
N_1-M	2.062	2.201	1.953	1.991
N_2-M	2.102	1.992	1.870	1.888
N_3-M	2.022	2.009	1.929	1.915
N_4-M	2.139	2.004	1.886	1.875
Cl_1-M	2.162	2.175	2.266	2.160
Cl_2-M	2.162	2.237		
		Bond angle		
N_1-M-N_2	94.327	85.358	97.521	97.037
N_2-M-N_3	78.702	81.004	84.159	85.347
N_3-M-N_4	95.728	92.793	98.485	92.381
N_4-M-N_1	78.627	79.553	85.011	86.086
N_1-M-N_3	86.640	84.879	140.449	123.854
N_2-M-N_4	171.345	164.160	110.319	103.685
N_1-M-Cl_1	87.539	88.087	86.605	94.162
N_2-M-Cl_1	93.624	94.574	109.227	118.367
N_3-M-Cl_1	169.980	171.962	85.792	87.096
N_4-M-Cl_1	91.108	89.745		
N_1-M-Cl_2	169.705	172.302		
N_1-M-Cl_2	93.984	97.226		
N_1-M-Cl_2	89.042	88.357		
N_1-M-Cl_2	92.528	97.148		
		Dihedral angle		
N_1-N_2-N_3-N_4	47.204	49.712	30.301	42.048

- Cl_1, Cl_2 and N_1, N_2, N_3, N_4 are belongs to chlorine and nitrogen atoms attached to the metal ion (M) in the bipy-phen complex

Table 4

Calculated Energy of HOMO and LUMO (in eV), HOMO-LUMO gap (ΔE_{H-L}, in eV), Global Hardness (η, in ev) and Global Softness (S, in eV)

Sample	E_{HOMO}	E_{LUMO}	ΔE_{H-L}	η	S
$[Fe(bipy)(phen)Cl_2]^+$	-0.563135	-0.542304	0.020831	0.010416	48.01
$[Fe(bipy)(phen)Cl_2]^+$-Y	-0.420351	-0.404554	0.015797	0.007898	63.30
$[Ni(bipy)(phen)Cl]^+$	-0.463879	-0.434131	0.029748	0.014874	33.61
$[Ni(bipy)(phen)Cl]^+$-Y	-0.378830	-0.354480	0.024350	0.012174	41.07